Study on Traveling Performance for Variable Wheel-Base Robot Using Subsidence Effect

Daisuke Fujiwara and Kojiro Iizuka
Shibaura Institute of Technology/Functional Control Systems, Saitama, Japan
Email: {nb16107, iizuka}@shibaura-it.ac.jp

Daichi Asami, Takashi Kawamura and Satoshi Suzuki
Shinshu University/Textile Science and Technology, Ueda, Japan
Email: {16fs302d, kawamura, s-s-2208}@shinshu-u.ac.jp

***Abstract*—In order to traverse the Lunar and Martian surface, planetary exploration rovers, which is equipped with cylindrical typed wheels, has been required high traveling performance. However, the cylindrical wheels of conventional rovers are easy to sink or slip on loose soil. Therefore, the rovers cannot move forward or backward in order to escape from the corresponding severe areas. In this study, we focus on an inching worm locomotion method to solve such a problem. The inching worm locomotion is a method that utilizes bearing force, which is generated between the ground and wheel when the wheel shears the ground. A few previous studies have investigated a method to traverse the loose soil. Further, a static sinkage was used to obtain bearing force in previous studies. This study proposes an advanced scheme that uses large sinkage to increase the traction. In order to confirm the effect of bearing force when the wheel sinkage is large, we performed traveling experiments on loose soil. From experimental results, the traveling performance of the robot, which is operated with the proposed scheme, indicated higher than that of the conventional scheme.**

***Index Terms*—inching worm locomotion, bearing force, loose soil, planetary rover**

I. Introduction

These days, many studies have been conducted into planetary exploration to the Moon or Mars. The NASA Mars mission in 1997 launched the rover Sojourner toward the Mars [1]. In 2003, NASA/JPL sent Mars Exploration Rover (MER) toward the Mars [2]. These rovers transmitted important scientific data back to the Earth. The purposes of the planetary exploration are to gather precise information and to investigate a wide range of rocks, soils, and clues to past water activity on the planet [3]. Moreover, a competition as Google Lunar XPRIZE in 2018 [4], [5] is taking place. In this competition, the rover needs to move on the Lunar surface. However, the Lunar or Martian surface contains loose soil and many steep slopes are located along the crater rims. Therefore, while traversing the loose soil, such rovers may easily slip and reach a poor condition. The rovers cannot move forward or backward in order to escape from the severe areas. In fact, the MER was sinking into the soil and could not move forward or backward in 2009. Therefore, the rovers are required high traveling performance to traverse the loose soil.

To avoid these problems, some previous studies have investigated an inching worm locomotion method to traverse the loose soil [6]-[9]. The inching worm locomotion is a method that utilizes bearing force, which is generated between the ground and wheel. Further, a static sinkage was used to obtain bearing force. In this study, we propose an advanced scheme that uses a large sinkage to increase the traction and confirm the effect of wheel's subsidence on traveling performance.

II. Method of Using Bearing Force and Mechanism of Generating Bearing Surface

A. Using Bearing Force in Conventional Inching Worm Locomotion Robot

Fig. 1 shows a conventional sequence of the inching worm locomotion [6]-[9]. From Fig. 1 in step1, when a robot travels forward direction, the static wheel pushes soil beneath the wheel toward backward and an embankment is generated. In this motion, the embankment supports the static wheel. Then the static wheel pushes the other wheel. Therefore, the embankment is considered as a bearing surface and plays an important role in the inching worm locomotion.

B. Mechanism of Wheel Sinking

In this section, a wheel sinking mechanics is explained. Interaction mechanics between soil and a wheel are investigated in terramechanics [10]-[13]. Fig. 2 shows the schematic diagram of a wheel sinking mechanism. Fig. 2a shows a static sinkage of a wheel and Fig. 2b shows a dynamic sinkage of a wheel. When a robot travels on a loose soil, a wheel slips or sinks. In terramechanics, a wheel sinkage is defined as a static and dynamic. The static

Manuscript received April 9, 2018; revised February 14, 2019.

doi: 10.18178/ijmerr.8.2.233-238

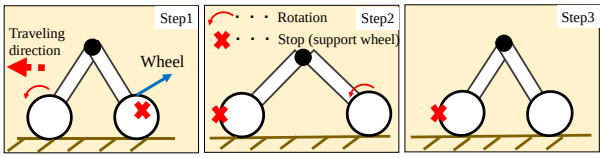

Figure 1. Sequence of the inching worm locmotion.

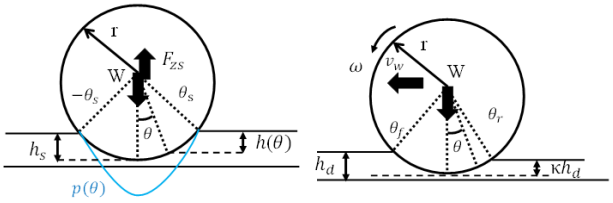

(a) Static sinkage. (b) Dynamic sinkage.

Figure 2. Sequence of the inching worm locomotion.

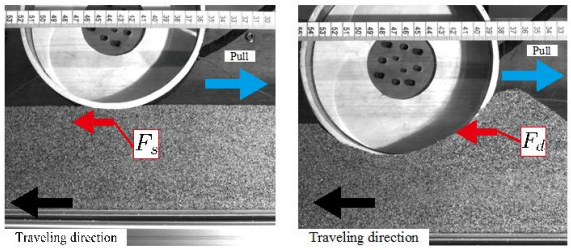

(a) Bearing surface is generated by the static sinkage.

(b) Bearing surface is generated by the deep sinkage.

Figure 3. Wheel is supported by bearing force.

sinkage h_s indicates that the sinkage is generated by normal force of a wheel without a wheel rotation. The dynamic sinkage h_d indicates that the sinkage is generated by rotating a wheel with arbitrary slip ratio. From these sinkage, the sum of the wheel sinkage h_a is showed as follows:

$$h_a = h_s + h_d \tag{1}$$

C. Using Large Bearing Force Generated by Large Sinkage

Fig. 3 shows images of wheel sinkage and these images are obtained by high-speed camera.

When a robot is operated with inching worm locomotion, a stationary wheel can get bearing force from backward surface, which is developed by the static sinkage (Fig. 3a). Meanwhile, when a wheel rotates depending on arbitrary slip ratio, the wheel sinks into sand. In this situation, the wheel can get bearing force from the deeper sinkage of the backward wheel (Fig. 3b). If a wheel rotates by large slip ratio, soil beneath the wheel moves into backward of the wheel as shown in Fig. 3b. Therefore, the deeper sinkage generates large bearing surface than the static one.

According to the equation formulated by soil mechanics [14], when a wall pushes soil mass, its reactive pressure is earth passive pressure P_p kN/m. As shown in Fig. 4, earth passive pressure P_p kN/m is given by the following:

$$P_p = W\tan(\varphi+\omega) = \frac{1}{2}\gamma_t H^2\left(\frac{\tan(\varphi+\omega)}{\tan\omega}\right) \tag{2}$$

Where W kN/m is soil mass of triangle mass, γ kN/m ^{3}is a unit weight and H m is height of a wall. Also, φ ° represents internal friction angle and ω ° represents angle formed by slip surface and ground surface. To obtain

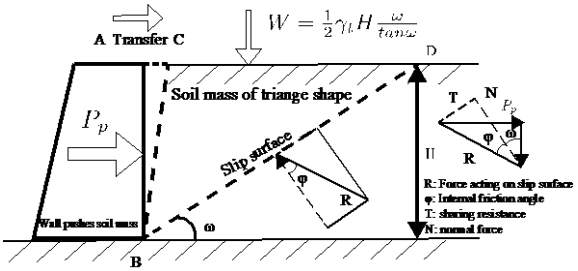

Figure 4. Schematic view of passive earth pressure.

bearing force, passive earth pressure is multiplied by bearing area.

According to (2), P_p kN/m increases with the wall height H m. Bearing force of a backward wheel increases with increasing a wheel sinkage. Therefore, the relationship of bearing force between the static and dynamic sinkage then indicates as follows:

$$F_s < F_d \tag{3}$$

Where F_s N indicates bearing force when a wheel sinkage is static (Fig. 3a). F_d N indicates bearing force when a wheel sinkage is deep (Fig. 3b).

III. Proposed Inching Worm Locomotion

A. Test Bed Robot

In this research, a variable wheel-base robot is used for traveling test. A variable wheel-base robot is shown in Fig. 5 , 6 and specifications of the robot are indicated in Table 1. The robot size is 410 mm width, 555 mm length and 390 mm height. The robot's mass is set to 10 kg. The wheel has a width of 40 mm and a diameter 170 mm. The wheel-base of the robot can change from minimum 170 mm to max 366 mm.

B. Proposed Traveling Sequence of the Test Robot

This robot is equipped with a variable wheel-base mode (an inching worm locomotion mode); the robot travels while changing wheel-base length and using large bearing force, which is generated by large sinkage.

TABLE I. The Specification of the Robot.

Robot size [mm]	W410 × L555 × H390
Robot weight [kg]	10
Wheel-base variable size [mm]	170-366
Wheel size [mm]	170

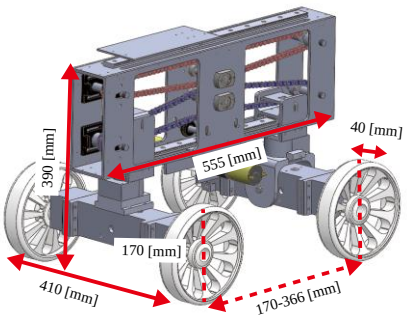

Figure 5. The test robot (CAD).

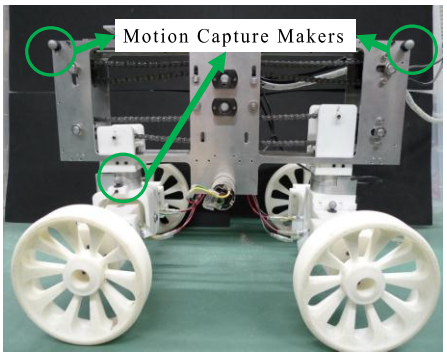

Figure 6. The test robot with motion capture makers.

The motion sequence of the robot, which is operated with the variable wheel-base mode, is shown in Fig. 7. Explanation of the motion as follows:

Motion 0: Static situation on loose soil with slope (Fig. 7a).

Motion 1: The front wheels rotate. The rear wheels stop (Fig. 7b).

Motion 2: The wheel-base is shortened. (The robot uses large bearing force from the backward of the front wheel then the robot shortens wheel-base. When the robot shortens wheel-base, the rear wheels rotate). (Fig. 7c).

Motion 3: The wheel-base is extended. (When the robot extends wheel-base, the front wheels rotate and the rear wheels stop). (Fig. 7d).

IV. Traveling Experiments

A. Experimental Environment and Conditions

The overview of the experimental system and experimental environment are shown in Fig. 8. The sandbox has a width, length and height of 485 mm, 2280 mm and 310 mm, respectively, and is filled with Keisa No.5 as loose soil. The longitudinal velocity and distance of the robot are obtained by a motion capture system (OptiTrack), which is set up outside the test field. The Motion capture markers are set upper of the robot (Fig. 6). To verify the locomotion methods using large bearing force of the wheel, traveling tests are performed using the variable wheel-base robot. In this study, two traveling methods are set. One is the rolling mode: The robot is driven using wheel rotation, the other is the variable wheel-base mode: The robot is driven changing wheel-base and using bearing force.

During the experiments, when the robot is operated with rolling mode, the wheel rotational speed sets at 1 rps and slope angles of the sandbox are set 0 °, 5 °, 10 °, 15 ° and 20 °. Meanwhile, when the robot is driven with the variable wheel-base mode, the wheel rotational speed set at 1 rps and slope angles of the sandbox are set 0 °, 5 °, 10 °, 15 ° and 20 °. The conditions of front wheel's sinkage are set as shown in Table 2. Each of the experimental conditions, experiments are carried out five times.

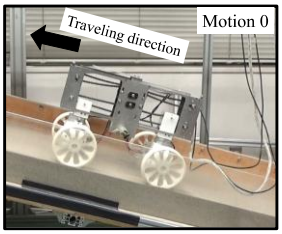

(a) Model: State of Motion 0.

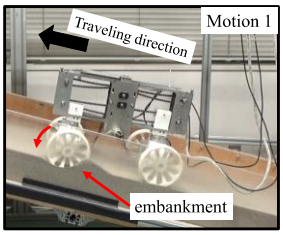

(b) Model: State of Motion 1.

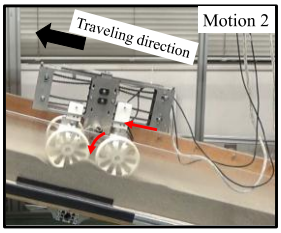

(c) Model: State of Motion 2.

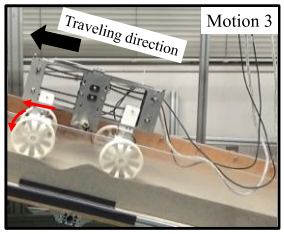

(d) Model: State of Motion 3.

Figure 7. Motion sequence of the robot.

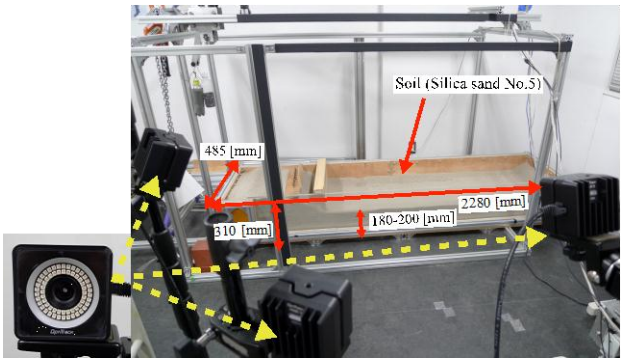

Figure 8. Overview of experimental setting for robot wheel test.

TABLE II. Experimental Settings of the Traveling Test; the Variable Wheel-base Mode.

Slope angel [°]	0, 5, 10, 15, 20				
Conditions	A (Static)	B	C	D	E
Sinkage [mm]	4.1 -18.3	25.7- 35.8	32.2- 41.1	36.8- 46.2	55.6- 73.1

B. Experimental Evaluation Index

1) Slip ratio of the rolling mode

When the robot is operated with the rolling mode on loose soil, the wheel generally slips. The traveling performance of the rolling mode is represented by the slip ratio s_r. It is expressed as follows;

$$s_r = 1 - x/X \quad (4)$$

Where x is actual traveling distance and X is distance when the robot travels on slope angle 0 ° with loose soil. If x is greater than X, the slip ratio has a value between 0 and 1. When the wheel moves forward without slippage, the slip ratio is 0; when the wheel does not move forward at all because of slippage, the slip ratio is 1.

2) Slip ratio of the variable wheel-base mode

When the robot is operated with the variable wheel-base mode, the front wheel generally slips form motion 1 to motion 2 (Fig. 7b-7c). The effectiveness of the variable wheel-base mode is represented by the slip ratio, s_{WB}. The slip ratio is expressed as with the rolling mode;

$$s_{WB} = 1 - x_{WB}/X_{WB} \quad (5)$$

As is the case of rolling mode, where x_{WB} is actual traveling distance and X_{WB} is distance when the robot travels on slope angle 0 ° with loose soil. If x_{WB} is greater than X_{WB}, the slip ratio has a value between 0 and 1. When the wheel moves forward without slippage, the slip ratio is 0; when the wheel does not move forward at all because of slippage, the slip ratio is 1.

V. Experimental Results and Disucussions

A. Rooling Mode

To analyze traveling performance of the rolling mode, we plotted the experimental results of the robot, which is operated with the rolling mode, on the graphs as shown in Fig. 9. Plotted data points in Fig. 9 represent the average value of the measured data acquired from five trials. The vertical axis indicates slip ratio and the horizontal axis indicates slope angles. According to Fig. 9, the robot of the rolling mode showed small slip ratio under slope angle 5 °. Meanwhile, slip ratio increased when the slope angles are greater than 10 °. In the experiments, we observed that the robot can travel when slope angles under 5 °. However, when slope angles were greater than 10 °, the wheels of the robot were stucked.

B. Variable Wheel-base Mode

Fig. 10, 11 show the experimental results of the robot, which is operated with the variable wheel-base mode. Fig. 10 shows the relationship between slope angles and sinkage of front wheels in motion 1 (Fig. 7b). Plotted data points in Fig. 10 represent the average value of the measured data. From Fig. 10, the sinkage increases with coming close to sinkage condition E.

Fig. 11 shows the relationship between the slope angles and slip ratio in each sinkage conditions. Plotted data points in Fig. 11 represent the average value of the calculated data from five trials. As shown in Fig. 11, under slope angle 10 °at all sinkage conditions, the slip ratio indicate under 0.6.

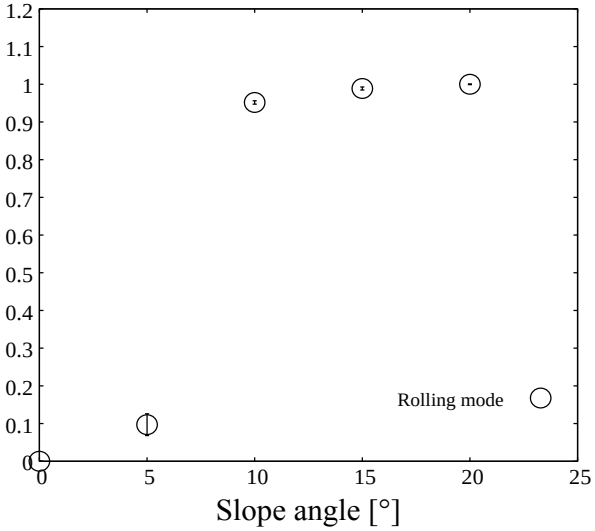

Figure 9. Relationship between slope angles and slip ratio. Therobot is operated with rolling mode. The bars show standard deviation (SD).

The slip ratio of sinkage conditions A (static sinkage) showed higher slip ratio on slope angles greater than 15 ° in comparison with sinkage condition B-E. Then, in sinkage condition A (static sinkage)-D, the slip ratio on slope angle 20 ° increased. However, in sinkage condition E, the slip ratio on slope angle 20 ° decreased. From these results suggest that the robot, which is operated with the variable wheel-base mode, has high traveling performance, especially over a steep slope. Moreover, larger sinkage of the wheel contributes to improving traveling performance of the robot.

VI. Conclusions

In order to verify traveling performance of the proposed scheme, we conducted traveling test using test robot, which is equipped with the variable wheel-base mechanism. Experimental results showed that the traveling performance of the variable wheel-base mode is higher than that of the rolling mode. Furthermore, in the variable wheel-base mode, we found that an increasing sinkage of the front wheel is a greater effect on the traveling performance, especially slope angles greater than 20 °. However, under slope angle 15 °, we confirmed that large sinkage of the front wheel decreases traveling performance. That is because large sinkage of the front wheel prevents extending wheel-base from motion 2 to motion 3 (Fig. 7c-7d).

As further studies, bearing force of wheel is necessary to evaluate traveling performance. Therefore, we will conduct single wheel tests. Form these tests, we will estimate the stress distribution and bearing force.

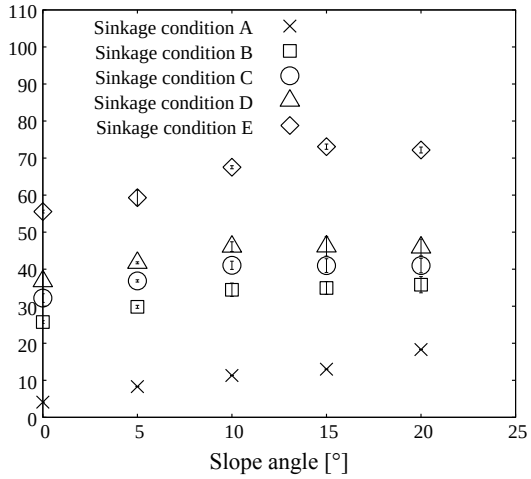

Figure 10. Relationship between slope angles and sinkage of the front wheels of the robot. The robot is operated with the variable wheel-base mode in motion 1. The bars show standard deviation (SD).

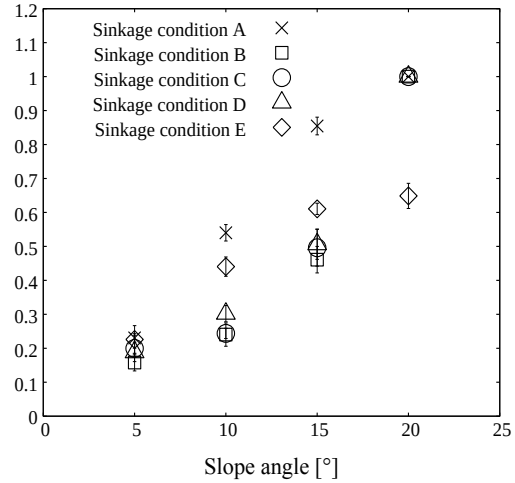

Figure 11. Relationship between slope angles and slip ratio. The robot is operated with the variable wheel-base mode. The bars show standard deviation (SD).

ACKNOWLEDGMENT

This work was supported by JKA and its promotion funds from KEIRIN RACE.

REFERENCES

[1] NASA/JPL, Pathfinder and Sojourner: 10 Years Later, Available: <https://www.nasa.gov/multimedia/imagegallery/image feature 861.html/>, (accessed on 30 December, 2017).
[2] NASA/JPL, Spirit & Opportunity Hightlights (2004), Available: <http://mars.nasa.gov/mer/home/>, (accessed on 6 July, 2017).
[3] I. Nakatani, T. Kubota and N. Yoshioka, "Rover for lunar, planetary exploration," *Journal of the Robotics Society of Japan*, vol. 14，no.7, pp. 940-943 1996.
[4] Google Lunar XPRIZE (2017), Available: <http://lunar.xprize.org/>, (accessed on 6 July, 2017).
[5] Hakuto (2017), Available: <https://team-hakuto.jp/>, (accessed on 6 July, 2017).
[6] D. Wettergreen, S. J. Moreland, K. Skonieczny, D. Jonak, D. Kohanbash, and J. Teza, "Design and field experimentation of a prototype lunar prospector," *The International Journal of Robotics Research*," vol. 29, no. 12, 2010.
[7] K. Skonieczny, S. J. Moreland, V. M. Asnani, C. M. Creager, H. Inotsume and D. S. Wettergreen, "Visualizing and analyzing machine-soil interactions using computer vision," *Journal of Field Robotics*, vol.31, no.5, pp.820-836, 2014.
[8] N. Patel, R. Slade, and J. Clemmet, "The ExoMars rover locomotion subsystem," *Journal of Field Robotics*, vol. 47, no. 4, pp. 227-242, 2014.
[9] C. Creager, K. Johnson, M. Plant, S. Moreland, and K. Skonieczny, "Push pull locomotion for vehicle extrication," *Journal of Terramchanics*, vol. 57, pp. 71-80, 2015.
[10] M. G. Bekker, *Off-The-Road Locomotion*, The University of Michigan Press, Ann Arbor, MI, USA, 1960.
[11] J. Y. Wong, and A. R. Reece, "Prediction of rigid wheel performance based on the analysis of soil-wheel stress: Part I. performance of driven rigid wheels," *Journal of Terramechanics*, vol. 4, no. 1, pp.81-98, 1967.
[12] M. G. Bekker, *Introduction to Terrain-vehicle Systems*, The University of Michigan Press, Ann Arbor, MI, 1969.
[13] J. Y. Wong, *Theory of Ground Vehicles*, John Wiley and Sons, 1978.
[14] K. Nishida, M. Hukuda, S. Takeshita, K. Yamamoto, K. Sawa, K. Saksaki and T. Nishigata, *Soli Mechanics*, Kajima institute publishing, 2015, p.129, (in Japanese).

Daisuke Fujiwara received his B.E and M.E degrees from Shinshu University, Japan, in 2011 and 2013, respectively. Since 2016, he has been with the Shibaura institute technology, Japan, where he is currently a Ph.D. student. His research development of an exploration rover for lunar and planet surface with rough terrain. He is a member of JSME and RSJ.

Kojiro Iizuka received his B.E. and M.E. degrees from Tokyo University of Agriculture and Technology, Japan, in 1997 and 1999, respectively, and Ph.D. (Eng.) degree from The Graduate University for Advanced Studies (SOKENDAI), Japan, in 2006. He joined Shinshu University as an Assistant Professor in Young Researchers Empowerment Project during 2008-2013 and then as an Associate Professor of Interdisciplinary Graduate School of Science and Technology during 2013-2016. In 2016, he joined Shibaura institute of technology, where his is currently an Associate Professor. His research interests include development of an exploration rover for lunar and planet surface with rough terrain. He is a member of JSME, RSJ and ISTVS.

Daichi Asami received his B.E degree from Shizuoka University, Japan, in 2016. He is currently an M.E. student at Shinshu University. His research interests include development of an exploration rover for lunar and planet surface with rough terrain.

Takashi Kawamura received his B.E., M.E., and Ph.D. (Eng.) degrees from The University of Electro-Communications, Japan, in 1987, 1989, and 1992, respectively. He joined Shinshu University in 1992, where he is currently an Associate Professor of Interdisciplinary Graduate School of Science and Technology. His research interests include intelligent and skillful robot systems. He is a member of JSME, IEEE and JSKE.

Satoshi Suzuki He received his M.E. and Ph.D. (Eng.) degrees from Chiba University, Japan, in 2006 and 2008, respectively. In 2009, he joined Shinshu University, where he is currently an Assistant Professor of the Faculty of Textile Science and Technology. His research interests include control of autonomous vehicle. He is a member of JSME, IEEE and RSJ.